

## Momentum spectra, charge ratio, and zenith-angle dependence of cosmic-ray muons\*

R. G. Kellogg and H. Kasha

*Physics Department, Yale University, New Haven, Connecticut 06520*

R. C. Larsen

*Physics Department, Brookhaven National Laboratory, Upton, New York 11973*

(Received 7 June 1977)

A large rotatable magnetic spectrometer was used to measure the sea-level energy spectra of cosmic-ray muons arriving at  $30^\circ$  and  $75^\circ$  zenith angle in the energy range 50–1700 GeV. The measured muon charge ratios and the ratio of the intensities at the two angles imply that the fraction of neutrons in the primary flux at energies above 1 TeV/nucleon is much larger than observed at lower energies and possibly as high as 25%.

### I. INTRODUCTION

High-energy muons at sea level, a debris of the interactions of high-energy primary cosmic rays with the air atoms' nuclei high in the atmosphere, carry information on both elementary-particle interactions at high energies and the nature of the primaries. The muons have been studied extensively in the atmosphere and underground (see Ref. 1 for a review). While the underground measurements extend to higher muon energies, they suffer from the uncertainties and fluctuations in the muon interaction with the rock. The sea-level measurements are limited by the resolving power and apertures of the spectrometers used. We have attempted to extend the range of muon measurements in the atmosphere<sup>2</sup> by constructing a large rotatable high-resolution magnetic spectrometer at Brookhaven National Laboratory, which was then used to measure the muon spectra at  $30^\circ$  and  $75^\circ$  zenith angle and their charge ratio.

Section II describes the spectrometer, its characteristics, and performance. Section III deals with the experimental runs, data reduction, and analysis. The measured charge ratio and angular distribution are discussed in Sec. IV in terms of their implications concerning the primary cosmic-ray flux. A model of muon generation consistent with the data is outlined in the Appendix.

### II. APPARATUS

#### A. General characteristics

The steepness with which the muon flux falls off with energy imposes definite requirements on the techniques of measurement. Assuming a canonical aperture of one m<sup>2</sup>ster, the rate of muons with energies greater than 1000 GeV is only 120 per

day. However, a total muon rate of  $1.2 \times 10^6$  per day can be expected above 10 GeV. Thus, measurements of muons with energies in excess of 1000 GeV are faced with "backgrounds" of the order of  $10^4$ . We have therefore employed a momentum selective trigger utilizing a scintillation-counter hodoscope.

Another problem which has to be faced in the design of a high-energy muon spectrometer is the attainment of sufficient momentum resolution. It is conventional to define a "maximum detectable momentum," or MDM, of a spectrometer as that momentum which corresponds to the root mean square measurement error in the magnetic bending angle (though some authors use the probable error, obtaining "larger" MDM's). Although it is possible to calculate correction factors to take these distortions into account, the corrections for momenta in excess of the MDM are necessarily dependent on detailed knowledge of the shape of the angular error distribution, and also assumptions concerning the actual shape of the momentum spectrum. The tails of the angular error distribution are particularly important in determining the corrections and are particularly hard to assess. The angular resolution necessary to extend muon momentum measurements beyond 1000 GeV is considerable. Taking a canonical magnetic field integral of 10 kG m, a 1000-GeV muon will be deflected only 0.3 mrad, which amounts to a displacement of 3 mm along a path length of 10 m.

A third problem, specific to our interest in determining the angular variation of the muon flux, was the necessity of reducing systematic errors between measurements conducted at different angles. It was clearly desirable to use the same instrument for the different measurements, but the resulting problems in maintaining critical

alignments over the length of a rotatable spectrometer required careful construction and design.

### B. Spectrometer

The spectrometer was based on a standard 18-in.-wide  $\times$  72-in.-long Brookhaven bending magnet modified by increasing its original 6-in. gap to 30 in. and filling the pole gap with a steel plug. The resulting magnet had a field uniform to within 2.5% and a field integral of 45.1 kG m at the operating current of 2.5 kA. At this current, the field in the center was 23.9 kG. The magnet, which weighed about 60 tons, was suspended 14 feet above the floor on a steel chassis. The magnet was attached to its supports by means of bearings which allowed it to pivot on a horizontal axis. Aluminum and steel frameworks were then attached to the front and back of the magnet to hold the other parts of the instrument — the spark chambers, trigger hodoscopes, cameras, and mirror system — in a fixed relationship as the spectrometer was rotated. The total length of this assembly was about 8 m, and it was roughly 2.5 m  $\times$  2.5 m in cross section. A  $\frac{1}{2}$ -horsepower electric motor, appropriately geared down, rotated the spectrometer from vertical to horizontal in about a minute. Figure 1 is a general view of the spectrometer, showing the arrangement of its various parts.

The ratio of the transverse momentum imparted

to a muon by the magnetic field at the operating value to the average transverse momentum imparted to the muon as a result of multiple Coulomb scattering in the steel of the magnet was 8.8:1 (independent of the muon momentum). Thus, we had an error of 11.4% in our momentum measurements due to this cause alone.

The spectrometer employed optical spark chambers 1 m (bending view)  $\times$  1.5 m in area. The plates consisted of 1-mil-thick aluminum foil stretched on aluminum frames. The spark gaps were 9.5 mm wide. The chambers were filled with helium at atmospheric pressure. A 10-kV pulse was applied using ceramic hydrogen thyratrons. Six identical spark chambers, each having 4 spark gaps, were used in all. Three of the chambers were placed in front of the magnet and three were placed behind. The spacing between chamber centers in each group of three was 36 in., giving a potential rms error in the magnetic bending angle of 0.55 mrad, if sparks formed in all the gaps and the hoped for spatial resolution of 0.5 mm for individual sparks was achieved. An extensive system of fiducials was adopted to achieve the required resolution by eliminating the effects of optical distortions. To this end fiducial bars were constructed to lie along the face of each chamber. Each bar consisted of a narrow aluminum strip to which light-emitting diodes were affixed, at accurately measured 2-in. intervals. Thus, no

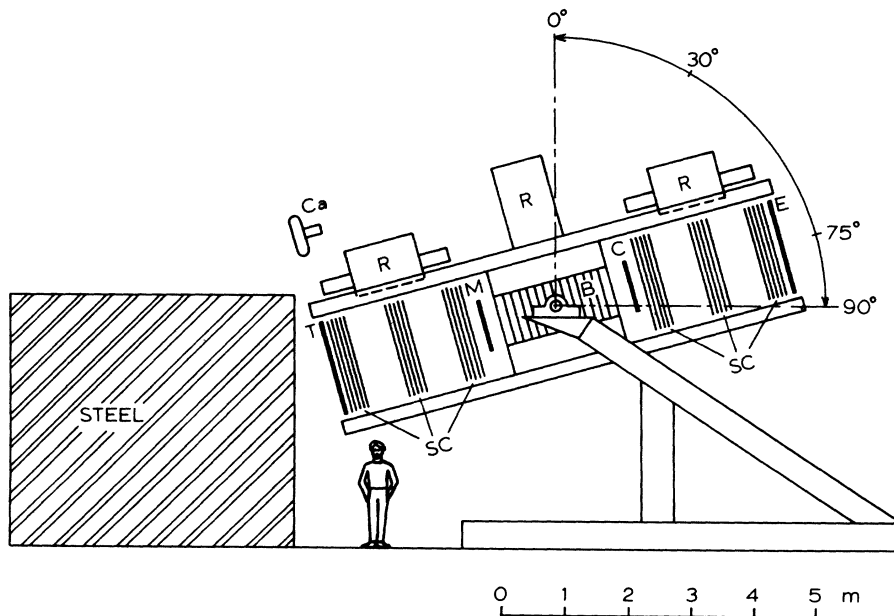


FIG. 1. Schematic elevation view of the spectrometer inclined at 75° to the zenith. SC: spark chambers, B: magnetic-field region, E, C, M, and T: scintillation-counter arrays, R: mirror boxes for the top view, Ca: camera. The steel absorber behind the spectrometer was used in the alignment and calibration procedure (see text).

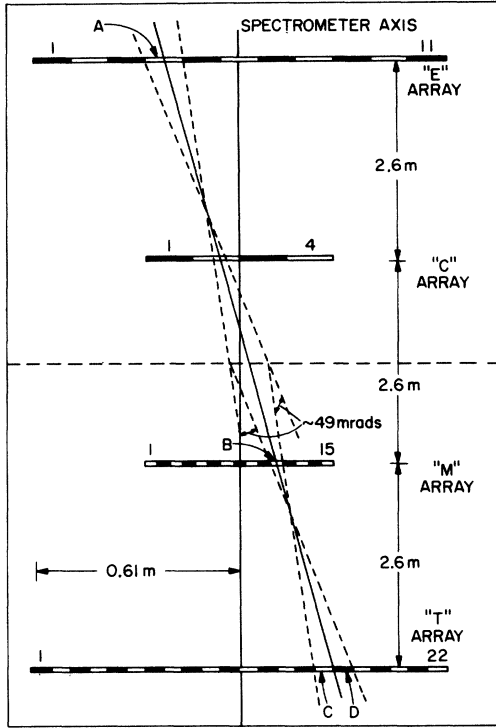


FIG. 2. Diagram of the hodoscope trigger.

spark was ever more than an inch in the crucial transverse direction from a point of known position.

The decision to use optical spark chambers was influenced by the existence of a computer-controlled film scanner at Brookhaven which was capable of measuring a frame of film in about 5–8 sec (one stereo view). In order that our production of film should not greatly exceed our ability to analyze it, it was imperative to hold the total trigger rate down by triggering selectively on high-energy muons. Without momentum selection,

the spectrometer would be sensitive to muons with energies greater than about 10 GeV, lower-energy muons being swept out of the aperture by the magnet. The trigger rate of such a nonselective instrument would be about one in 3.5 sec when pointed at a zenith angle of  $30^\circ$ . The momentum-selective trigger which we devised raised the half-efficiency momentum from 10 GeV to 50 GeV and reduced the trigger rate by about a factor of 25. The trigger system consisted of four hodoscope counter planes (*E*, *C*, *M*, and *T*, Fig. 1). The planes *E* (11 counters) and *T* (22 counters),  $1 \times 1.5$  m in size, were placed at the two extremities of the spectrometer at  $\pm 3.66$  m from its center. The planes *C* and *M*,  $0.46 \text{ m} \times 0.76 \text{ m}$  in size, consisting of 4 and 15 counters, respectively, were straddling the magnet at  $\pm 1.22$  m from its center. In all trays the counters were parallel to the field lines so that the magnet would sweep muons across their narrow dimensions. The counters were made of Pilot Y scintillator 0.5 in. thick and employed RCA 8575 photomultiplier tubes. A diagram of the trigger system can be found in Fig. 2. The *E*, *M*, and *T* trays comprised the momentum selecting part of the trigger, the *C* tray was used only to require that a particle had passed through it in time coincidence. The geometrical arrangement was such that the very apex of the penumbra of any pair of *E* and *M* counters fell at the dividing line between two *T*-tray counters, and the umbra extended over these two, and only these two, *T*-tray counters. If a muon passed through a given *E* counter and a given *M* counter, a trigger would be generated only if it passed through either one of the two shadowed *T*-tray counters as well. In this way all particles passing through the geometrical aperture of the spectrometer in a straight line would be seen, but the trigger would become increasingly inefficient the more a particle was deflected by the magnet. Because of the inverse relation of deflection and momentum, the result-

TABLE I. Characteristics of the spectrometer's aperture.

Aperture for undeflected particle	$A_0 = 146 \text{ cm}^2 \text{sr}$
Momentum dependence of aperture ( $p$ in GeV)	$\frac{A}{A_0} = \begin{cases} 1 - \frac{1}{2}(55/p)^2 & p \geq 55 \text{ GeV} \\ \frac{1}{2}(55/p - 2)^2 & 27.5 \leq p \leq 55 \text{ GeV} \\ 0 & p < 27.5 \text{ GeV} \end{cases}$
Relative aperture for different entrance angles	$A(x, y, q) = f_x(x) f_y(y) A(p)$ $f_x(x^\circ) = \begin{cases} (17.35^\circ - x)/254, & x \leq 8.9^\circ \\ (11.8^\circ - x)/86.6, & 8.9^\circ \leq x \leq 11.8^\circ \end{cases}$ $f_y(y^\circ) = \begin{cases} (10.6^\circ - y)/102, & y \leq 6.5^\circ \\ (7.9^\circ - y)/34.2, & 6.5^\circ \leq y \leq 7.9^\circ \end{cases}$
Half of the total aperture is within $4.1^\circ$ zenith angle of the spectrometer axis.	

ing momentum cutoff in the aperture was quite sharp; the relative acceptance being 90% at 100 GeV, 50% at 55 GeV, and zero at 27 GeV. The effective aperture for different momenta is given by the formula in Table I.

Also given in Table I is the manner in which the relative aperture falls off as a function of angle away from the spectrometer axis. The spectrometer when pointed at zenith angle  $Z$  will observe particles with incident zenith angles in the range  $Z \pm 11.8^\circ$ . The acceptance is peaked at the center, however, and half of it lies in approximately the central third of this range, in the interval  $Z \pm 4.1^\circ$ . Since the muon flux at inclined angles is a strong function of zenith angle, this finite width of the angular acceptance must be taken into account when the results are analyzed.

### C. Momentum resolution

Definitive measurements of the spectrometer's resolution rested upon a series of runs undertaken especially for the purpose. In these runs, which were made periodically during the course of the experiment, the normal trigger of the spectrometer was altered to select muons which passed through the air gaps of the magnet (see Fig. 3) and through 5 m of steel placed behind the spectrometer. Since the effective energy of the muons which successfully passed through the steel was 8 GeV, they could be expected to acquire a scattering angle distribution with a standard deviation of 0.4 mrad in passing through the residual matter

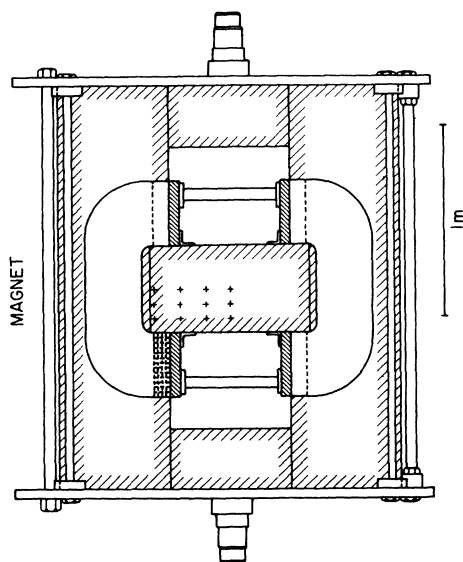


FIG. 3. Cross section of the magnet perpendicular to the spectrometer axis.

of the spectrometer and the fringing field of the degaussed magnet. Any extra width in the measured bending-angle distribution of these muons could then be attributed to the finite resolution of the spectrometer.

When the "straight-through" film was measured with the automatic measuring machine, the measured bending angles had a  $\sigma_{\text{meas}} = 1.2$  mrad. When the same film was measured by hand on a conventional measuring table,  $\sigma_{\text{meas}}$  dropped to 0.9 mrad. Since

$$\sigma_{\text{meas}} = (\sigma_{\text{scat}}^2 + \sigma_{\text{res}}^2)^{1/2},$$

where  $\sigma_{\text{scat}} = 0.4$  mrad is the standard deviation of the scattering angle and  $\sigma_{\text{res}}$  is the standard deviation of measurement errors due to the resolution of the measurement process, we find that  $\sigma_{\text{res}} = 1.13$  mrad for the automatic machine and  $\sigma_{\text{res}} = 0.81$  mrad for the conventional measuring table. The momenta corresponding to these angles are the MDM's associated with each method of measurement. The MDM is therefore 1700 GeV for hand-measured events and 1200 GeV for events measured by the automatic machine. The bulk of the noncalibration data was of course scanned by the automatic machine, but all muons which were found in this way to have momenta greater than 500 GeV were later remeasured by hand, so that the effective MDM of our measurements is 1700 GeV.

Because of the steepness of the muon spectrum, uncertainties in the momentum measurements of individual particles will cause more muons to be incorrectly assigned energies above an arbitrary threshold energy than to be incorrectly assigned energies below the threshold. This effect leads to an overestimate of the muon intensity which is proportional to the spectral exponent. For a momentum uncertainty of 11.4%, however, this error is small. Even in the steepest region of the muon spectrum, where the exponent is about 3.5, the resulting overestimate of the intensity is only 2.5%.

Another, more subtle, distortion caused by introducing the iron plug into the path of the muons is produced by the possibility that a muon will create an electromagnetic shower in the plug which had sufficient energy to escape. These showers have the ability to swamp the chambers beneath the magnet and render measurement of the muon momentum impossible. Since the probability for energetic shower production increased with muon energy, this effect creates a bias against high-energy muons. Calculations show that for energies less than 1000 GeV, muon bremsstrahlung and direct pair production are primarily responsible for producing such showers and that the bias introduced against 1000-GeV muons is likely to be about 7%.

### III. DATA TAKING AND REDUCTION

#### A. Choice of zenith angles

The range of zenith angles toward which we could point our spectrometer extended from  $0^\circ$  (for vertical muons) to  $90^\circ$  (for horizontal muons); however, various considerations led us to concentrate our measurements at  $30^\circ$  and  $75^\circ$ . A rough analysis, which predicts all the essential features of the muon flux correctly, gives the angular dependence of muon production in the atmosphere as

$$\frac{1}{1 + E/E_c \sec \theta'}$$

where  $E$  is the muon energy,  $E_c$  is the critical muon energy which depends on the type of meson from which muons have decayed, and  $\theta'$  is the angle, at the effective height of muon production, between the zenith vector and the trajectory of the muons.  $\theta'$  differs significantly from  $\theta$ , the similar angle at the point where the muons reach the ground, only for nearly horizontally incident muons, such that  $\theta$  approaches  $90^\circ$  (Fig. 4). Since pions strongly dominate over kaons, we can consider  $E_c$  to be equal to the pion critical energy of 92 GeV. We see then that at any energy the muon production is an increasing function of  $\theta'$ , and in the limit that  $E$  is much greater than  $E_c$ , the muon production increases directly as  $\sec \theta'$ . After their production, of course, muons are subject to energy losses and to the possibility of decay. Since both the decay path length and thickness of energy absorbing atmosphere are greater for sloping muons than for more nearly vertically incident ones, these flux reducing effects are increasing functions of  $\theta$ . Likewise, the larger the muon energy, the smaller is the fraction of its energy which is lost in passing through the atmosphere and the smaller is its probability for decay

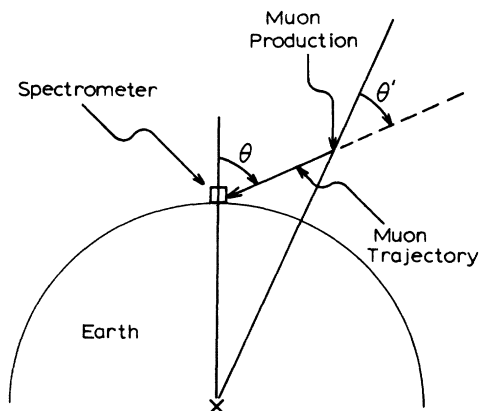


FIG. 4. Muon production geometry.

in flight. These effects are therefore decreasing functions of  $E$ . It can be reasoned then that the flux of muons of a given energy reaching the earth will increase as a function of  $\theta$  until such point as the flux reducing effects of energy loss and decay more than compensate for the increasing muon production. There exists, therefore, an angle at which the flux of muons of a given energy is maximum, and this angle is an increasing function of muon energy.

For muon energies well above the critical energy, the effects of muon energy loss and decay are small enough so that the angle of maximum muon flux is determined primarily by the "saturation" of  $\theta'$ . Up to a zenith angle of  $80^\circ$ ,  $\theta$  and  $\theta'$  are essentially equal, but at this point  $d\theta'/d\theta$  begins a rapid decrease and, while  $\theta$  increases to  $90^\circ$ ,  $\theta'$  approaches a maximum of  $86.15^\circ$ , where the secant is 14.9 rather than infinity. Therefore, at large zenith angles the rapid increase in muon production with zenith angle flattens off. The flux-reducing effects, however, continue to grow as strong functions of the zenith angle. The result is that the angle of maximum muon flux is essentially constant for muon energies above 1000 GeV at a value of about  $87^\circ$ , where  $\theta'$  is  $85.1^\circ$  and  $\sec \theta'$  is 11.8.

Considering this saturation of the muon flux angular dependence, and considering the finite width of our spectrometer's angular acceptance, it was decided to point the spectrometer at  $75^\circ$  in order to accumulate data for large zenith angles.

At the other end of our angular range, toward the vertical, the variation in  $\sec \theta$  and, hence, the muon flux is very gradual. We therefore decided to make our measurements at  $30^\circ$ , where the secant is 1.15, rather than at the vertical, where it is 1.0, not because of any difference in the muons, but because of differences in the interference we expected from extensive air showers. Muons, and especially high-energy muons, are not likely to reach the earth totally unaccompanied. Rather, they are just one component of the extensive air showers produced by the primary particles. The main constituents of these showers, as far as numbers of particles is concerned, are electrons and photons which arise from the decay gammas of neutral pions just as the muons arise from the decay of charged mesons. At ground level, the electrons in a typical shower outnumber the muons by a factor of 10. Because of the highly relativistic nature of all the particles involved, the entire air shower arrives within a very short period, about 10 nsec, and it is clear that the lateral separation of the particles should be large compared to the size of our apparatus if the spark

chambers are not to be saturated with the tracks of many electrons whenever a muon triggers the spectrometer. The radial extension of air showers is, however, in the neighborhood of 60 m, so that a considerable number of shower particles can be tolerated before their density becomes large enough to interfere with our measurements, and in fact the overwhelming majority of the muons we observed traversed the spectrometer unaccompanied.

However, it must be remembered that high-energy muons will come preferentially from high-energy primaries which also produce large air showers. Also, because of the invariant nature of the transverse-momentum distribution of produced mesons, higher-energy muons are likely to fall closer to the shower axis where the electron density is greatest. Clearly these showers then introduce a bias against high-energy muons which might not be apparent from the data because the high-energy muons are themselves so rare. Calculations indicate that perhaps 30% of all 2000-GeV muons incident from the vertical would be accompanied by electron densities large enough to make them impossible to observe with our spectrometer (see Bennett and Greisen<sup>3</sup> for measurements of the distribution of muons in extensive air showers).

Unlike the muons, however, which pass through the atmosphere almost unaffected, the electromagnetic showers are being attenuated as they reach the surface of the earth. By taking advantage of the 15%-thicker atmosphere layer available at a zenith angle of 30°, our calculations show that only about 5% of 2000-GeV muons will be obscured by excessive electron densities. Also, the obscuring effects of showers drops off rapidly as the muon energy is reduced. Compared to muons of 2000 GeV, muons of 1000 GeV will be lost only  $\frac{1}{10}$  as often, in other words only 0.5% will be obscured at 30°.

While these considerations show that a vanishingly small proportion of all muons incident on the spectrometer will be obscured by showers, it is nevertheless true that about half the triggers of the spectrometer were caused by electromagnetic showers rather than muons. Since the momentum-selecting trigger did not reject events that fired a great number of the hodoscope counters, extensive air showers could trigger the spectrometer simply by hitting a large number of counters and satisfying the straight-line requirement by chance. The particle density required to produce such a random trigger is estimated as about 10/m<sup>2</sup>, and in fact the rate of showers depositing such densities on the spectrometer is consistent with our rate of triggers due to showers.

### B. Experimental runs

Over a period of about two years we operated our spectrometer to observe muons incident from 30° and 75°, splitting up the time so as to record approximately equal numbers of muons at the two angles. In all, 400 000 events were recorded on about 50 000 feet of film. At 30° the total trigger rate was 84/hour which required us to load new 100-ft rolls of film twice a day, while at 75° the trigger rate dropped to 42/hour and the film required changing only once a day. Table II indicates how these total trigger rates were distributed among muons, muons which interacted in the magnet plug and extensive air showers. These rates were obtained by hand examination of about 2500 events, and the categorizations above proved to be clear and unambiguous. Events classified as muons in general showed a single unaccompanied track, although the tracks of  $\delta$  rays and the remains of weak air showers were not allowed to disqualify otherwise unambiguous tracks. Since the tracks all passed through at least substantial portions of the magnet plug without a sign of interaction, their identity as muons rather than electrons or hadrons is well established. Events classified as muons interacting in the magnet, or muon showers, showed single tracks entering the spectrometer and sprays of tracks exiting beneath the magnet plug. The identity of these particles as muons is highly probable. All but very-high-energy — and therefore rare — hadrons would be absorbed totally in the magnet plug. Events classified as extensive air showers showed a great number of scattered sparks in the chambers and often had fired a majority of the hodoscope counters.

It will be noticed that the trigger rate for all categories declines in going from 30° to 75°. That the muon enhancement we expect at 75° is not apparent is due to the fact that the total muon rate is dominated by muons of low energy. The pions producing these muons had a substantial probability to decay even at 30° so that the zenith-angle

TABLE II. Categorization of events triggering the spectrometer. 25% of the muons triggering the spectrometer were later rejected because their trajectories failed to lie wholly within the steel plug of the magnet. For each entry, we give the rate/hr and (in parentheses) the percent of the total.

Angle	Muons	Muons interacting in magnet	Extensive air showers
30°	34 (40%)	2.5 (3%)	48 (57%)
75°	21 (51%)	1.3 (3%)	19 (46%)

enhancement effect is fairly well saturated. Furthermore, the flux-reducing effects of muon decay and muon energy loss affect the muons coming from  $75^\circ$  a great deal more than those coming from  $30^\circ$  because of their much longer path length in the atmosphere. Therefore, the total flux of muons above something like 50 GeV, which is what the muon trigger rate of the spectrometer measures, is substantially less at  $75^\circ$  than at  $30^\circ$ .

The observation that the rate of muons interacting in the magnet steel declines even more than the total muon rate in going from  $30^\circ$  to  $75^\circ$  is a clue to the nature of these muons. Only about 7% of even 1000-GeV muons are expected to produce visible showers, and this number drops rapidly with decreasing energy. Muons of 50 GeV can be expected to shower about 1% of the time, and weighing these probabilities appropriately with the muon spectrum, we could expect somewhat less than 2% of all muons with energies above the spectrometer's cutoff to shower. However, of all muons triggering the spectrometer, the fraction observed to induce showers was 5%. The abundant muons with energies below the cutoff of the spectrometer can trigger the instrument if they shower in the magnet, however, and spray the rear hodoscopes with electrons. The fact that the rate of such muons below cutoff drops more substantially than the total muon trigger rate in going from  $30^\circ$  to  $75^\circ$  is, of course, reflected in similar behavior of the interacting muon rate. Calculations show that the flux of muons below cutoff and their probability for producing showers can account precisely for our observed rates.

Air shower triggers also show a great decline from  $30^\circ$  to  $75^\circ$ . This is due not so much to the change in the intensity of showers coming from these directions, but rather to the characteristics of the trigger system's time resolution. The decline in the shower rate as a function of angle is so abrupt in fact, that for our purposes, all showers can be assumed to come from the vertical. The decline in the rate of showers triggering the apparatus when it is rotated from  $30^\circ$  to  $75^\circ$  can be explained entirely by the amount vertically incident shower particles striking the  $T$  tray and the  $E$  tray become further out of time as the spectrometer is rotated toward the horizontal.

### C. Data reduction

We scanned and measured the film on a computer-controlled scanning machine. The machine was instructed to search along the locations of the spark-chamber gaps for sparks after it had oriented itself on the film using the extensive fiducials recorded, and a careful search was made of the

other gaps in the chamber immediately above and below the gap in which the spark was found. In this way, the sparks were organized efficiently into track segments passing through each chamber. When all chambers of a given frame had been searched in such a manner, the coordinates of the sparks organized into chamber segments and the coordinates of the neighboring fiducial lights were written on magnetic tape. The machine then advanced to the next frame and commenced in a similar fashion. Towards the end of the scanning project, when time was important, the scanning machine was operated 24 hours a day, largely without supervision.

The measuring accuracy and resolution of the machine appeared to be adequate. If a straight line was fit to the four sparks of a particle passing through a single chamber, the corrected rms deviation of the sparks from the line was equal to the digitization granularity of the machine. This in turn corresponded to an error in the actual spark locations of about 0.25 mm. Since the sparks recorded on film appeared to be about 10 mm wide on average, the centering accuracy of the machine is seen to be about one part in 40. When straight lines were fit between the track segments in different chambers, however, the apparent resolution of 0.25 mm could not be justified. The corrected rms displacement of track segments from a straight line was found to be about 0.75 mm. When events were measured on a conventional measuring table, the resolution improved slightly.

The magnetic tapes generated by the scanning machine were processed by programs running on the CDC 6600 computers at Brookhaven. These programs associated the top- and side-view measurements of each event and fit straight lines to the sparks in the three chambers in front of the magnet and to the sparks in the three chambers behind the magnet. Checks were then made to assure that the muon had in fact passed through the hodoscope planes and that it had passed properly through the magnet plug. The ingoing line and the outgoing were then required to pass sufficiently close to each other at the center of the magnet and not to exhibit too much bending in the direction parallel to the magnetic field. These tests were designed to eliminate low-energy muons which had undergone large-angle scattering in the magnet in such a way as to mimic high-energy particles. Passing all cuts, the momentum of the muon was determined from the bending angle of the in and out lines in the plane perpendicular to the field. The muon momenta were histogrammed to provide the program's basic output and for each muon with momenta greater than 500 GeV the momentum was printed out along with the

TABLE III. Raw momentum distribution. The Roman numerals I and II denote the two magnet polarities, while the letters A and B denote the direction in which the muons were bent. The signs + and - then indicate the electric charge of the muons.

Momentum bin (GeV)	75°				30°			
	IA	IB	IIA	IIB	IA	IB	IIA	IIB
	+	-	-	+	+	-	-	+
50-63	860	392	348	244	917	422	872	629
63-80	743	427	303	284	662	384	729	611
80-100	555	342	230	239	406	286	470	420
100-125	430	314	136	170	283	176	319	286
125-160	314	251	128	154	214	140	225	228
160-200	186	142	69	92	126	93	124	117
200-250	146	83	49	67	80	48	79	86
250-400	172	127	69	76	70	47	86	70
400-∞	119	72	42	54	51	29	60	36

frame number of the event for later study.

As noted in Table II, about 25% of all muons failed to pass through the fiducial volume of the magnet properly. Most of these failed to remain wholly in the magnet plug, but some trajectories failed to reconstruct properly through the hodoscope trays. That muons produced triggers when apparently missing a hodoscope counter by an inch or so, we ascribed to the effects of  $\delta$ -ray electrons. Very few events contained tracks which bent excessively in the direction parallel to the field or failed to meet at the center of the magnet. Although the program was capable of handling events containing the tracks of more than one muon, no such events were detected.

The raw distribution of muon momenta obtained by analysis of the film is presented in Table III.

Because of small unavoidable misalignments in the positioning of the trigger hodoscope counters, the spectrometer was more efficiently triggered by muons which were deflected in one direction than in the other. Since the observed charge ratio will be very sensitive to such asymmetries, we had already taken care to accumulate approximately equal amounts of data in each polarity of the bending magnet. Although this precaution was likely to remove most of the distortions introduced by right-left asymmetries in the aperture, it was felt that a minimum amount of further analysis would be extremely efficient in eliminating any residual effects.

In order to arrive at a "self-consistent" measurement of the charge ratio, we made the assumption that the aperture,  $G$ , of the spectrometer is a function of the bending direction as well as the momentum of the particles. We then used the observed charge ratios in the two magnet polarities,  $R_I$  and  $R_{II}$ , to calculate both the "self-consistent"

charge ratio,  $R_{sc}$ , and the aperture asymmetry ratio,  $Z = G_a/G_b$ , which is the ratio of the apertures between the two bending directions,  $a$  and  $b$ . By means of this assumption, we have then

$$R_I(p) = R_{sc}(p)G_a(p)/G_b(p),$$

$$R_{II}(p) = R_{sc}(p)G_b(p)/G_a(p),$$

and by simple manipulation we obtain

$$R_{sc}(p) = (R_I R_{II})^{1/2},$$

$$Z(p) = G_a/G_b = (R_I/R_{II})^{1/2}$$

It was found that, although  $R_I$  and  $R_{II}$  are strong functions of momentum,  $R_{sc}$  shows little or no momentum dependence, just as the charge ratios found by other workers seem to be independent of momentum. Furthermore, the shape of  $Z$ , the aperture asymmetry ratio, as a function of  $p$ , is predicted well by assuming that the asymmetry of one of the apertures is caused by a displacement of one of the hodoscope trays. Allowing the position of the  $T$  tray to vary, we found by means of a least-squares fit to the 75° data that the aperture asymmetry is well explained by an effective  $T$ -tray displacement of  $0.28 \pm 0.02$  in. Figure 5 is a graph showing our measured values of  $Z$  for each momentum bin with a superimposed line predicting  $Z$  for a  $T$ -tray displacement of 0.28 in. Equipped with this explanation of the asymmetry, we felt that the charge ratios calculated above allowing the values of  $Z$  complete freedom would be more strongly influenced by statistical fluctuations than charge ratios calculated under the assumption of a 0.28-in.  $T$ -tray displacement. We therefore calculated the aperture for each momentum bin and bending direction relative to the aperture for undeflected particles under this assumption, and then corrected the raw momentum distribution of Table III by dividing the number of muons observed in each momentum bin and bending direction by the

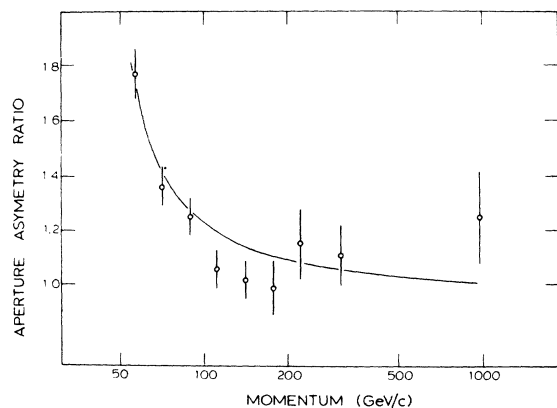


FIG. 5. Aperture asymmetry ratio as a function of the muon momentum.

TABLE IV. Momentum distribution after correction for the momentum and bending direction dependence of the aperture.

Momentum bin (GeV)	75°				30°			
	IA +	IB -	IIA -	IIB +	IA +	IB -	IIA -	IIB +
50-63	1298	1050	525	653	1384	1130	1316	1685
63-80	919	737	375	490	819	662	902	1054
80-100	621	480	257	335	454	401	526	589
100-125	456	394	144	213	300	221	338	358
125-160	323	293	132	180	220	163	232	266
160-200	188	158	70	103	128	104	126	130
200-250	147	90	49	73	80	52	79	93
250-400	172	134	69	80	70	49	86	74
400-∞	119	72	42	54	51	29	60	36

appropriate relative aperture. The resulting corrected momentum distribution can be found in Table IV, which represents the distribution of muons which would be observed by a spectrometer whose aperture is independent of both momentum and bending direction, and equal to the aperture of our spectrometer for undeflected muons.

#### D. Calculation of charge ratio

From these corrected data, calculation of the charge ratios was straightforward, and the results can be found tabulated in Table V and graphed in Fig. 6. We find no significant difference in the ratios calculated in this manner and the self-consistent ratios mentioned before. The uncertainty in determination of the  $T$ -tray displacement, and hence in the aperture weights, is reflected in these calculated charge ratios. Such uncertainties have an appreciable effect only on the lowest momentum bin.

TABLE V. Muon charge ratios.  $\chi^2$  is computed for the hypothesis that the muon charge ratio is not a function of momentum.

Momentum bin (GeV)	30°	75°	30° + 75°
50-63	1.25 ± 0.03	1.24 ± 0.04	1.25 ± 0.030
63-80	1.20 ± 0.03	1.27 ± 0.05	1.23 ± 0.032
80-100	1.13 ± 0.05	1.30 ± 0.06	1.20 ± 0.040
100-125	1.18 ± 0.07	1.24 ± 0.07	1.21 ± 0.049
125-160	1.23 ± 0.08	1.18 ± 0.08	1.21 ± 0.057
160-200	1.12 ± 0.10	1.28 ± 0.11	1.20 ± 0.076
200-250	1.32 ± 0.15	1.58 ± 0.17	1.46 ± 0.115
250-400	1.07 ± 0.13	1.24 ± 0.12	1.17 ± 0.087
400-∞	0.98 ± 0.15	1.52 ± 0.18	1.28 ± 0.120
50-∞	1.203 ± 0.020	1.267 ± 0.024	1.23 ± 0.015
$\chi^2$ (D.F. = 8)	9.37	7.52	6.11

#### E. Momentum spectra

The shapes of the muon momentum spectra at the two angles can also be found directly from the corrected data in Table IV but the absolute spectra and the ratio of the intensities at the different angles are not defined by this data alone. In order to measure these quantities, about 2500 events, divided between the two angles and recorded on successive days shortly after the spectrometer's trigger system had been thoroughly tested for efficiency, were scanned and measured by hand on a conventional measuring table. By basing our absolute measurements of the muon fluxes on these hand measurements, we achieved independence from fluctuations in the track-finding efficiency of the automatic measuring machine. Although the automatic machine found about 90% of all muon tracks when it was working properly, this effi-

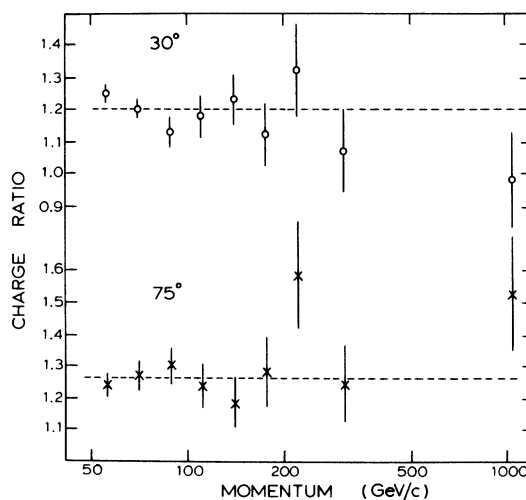


FIG. 6. Muon charge ratios at 30° and 75° as a function of the muon momentum.

TABLE VI. Results of hand-scanned events.

Roll number	741	742	743	744
Zenith angle	30°	75°	30°	75°
Trigger rate (sec <sup>-1</sup> )	0.023 60	0.011 75	0.023 39	0.011 58
No. of frames scanned	462	341	882	887
Measured muons	157	181	322	404
Muons lost due to measuring errors	42	2	12	34
Measuring efficiency	0.789	0.964	0.989	0.922
Average trigger rate		30°	0.023 49 ± 0.000 59 sec <sup>-1</sup>	
		75°	0.011 67 ± 0.000 29 sec <sup>-1</sup>	
Time that spectrometer was gated off for each event			$t = 2.09 \pm 0.02$ sec	
Trigger efficiency due to gate-off time		30°	0.9018	
		75°	0.9512	

ciency was prone to fluctuations, primarily in the negative direction from sources such as skipping frames or inability to locate a particular chamber, which were not expected to distort the spectral shapes but made determination of the absolute muon rates from the automatically scanned data an unsure procedure.

Most of the 2500 hand-scanned events underwent two scanning passes where on the second pass all events which had not been identified as electromagnetic showers or muon showers on the first pass but had, nevertheless, failed reconstruction by the analysis programs were scanned again. Then all of the 2500 events were screened by

physicists to ensure that any muon events slipping through this procedure would be properly accounted for. The disposition of the hand-scanned frames can be found in Table VI along with other information relevant to the determination of the absolute muon rates. Under the category "muons lost to measuring errors" are listed the muon events found in the final screening which had either been missed in the two previous passes (only two or three) or had failed reconstruction because of measuring-machine malfunction. Roll 741, which had not enjoyed the benefit of a second measuring pass, can be easily distinguished by its lower measuring efficiency which is cal-

TABLE VII. Corrected momentum distribution of hand-scanned events.

Momentum bin (GeV)	Roll Angle	741		742		743		744	
		30°		75°		30°		75°	
	Bending Charge	IIA	IIB	IIA	IIB	IIA	IIB	IIA	IIB
		-	+	-	+	-	+	-	+
50-63		12.1	26.8	24.2	24.1	39.3	58.9	52.8	64.3
63-80		12.4	12.1	12.4	20.7	32.2	29.3	30.9	39.7
80-100		6.7	7.0	6.7	11.2	14.5	18.2	26.8	46.3
100-125		5.3	5.0	3.2	10.0	11.7	12.5	13.8	18.8
125-160		1.0	9.3	10.3	10.5	3.1	7.0	7.2	12.8
160-200		3.0	4.5	2.0	4.5	3.0	1.1	12.1	17.8
200-250		1.0	0.0	2.0	6.5	3.0	4.3	2.0	13.0
250-400		1.0	1.1	2.0	4.2	3.0	1.1	6.0	9.5
400-∞		1.0	0.0	4.0	6.0	4.0	1.0	3.0	3.0
Roll total		109.3 ± 13.4		164.5 ± 15.5		247.2 ± 20.2		379.8 ± 24.2	
Scanning efficiency		0.789		0.964		0.989		0.922	
Efficiency-corrected total		138.5 ± 17.0		166.3 ± 15.7		256.2 ± 21.0		412.0 ± 26.2	

TABLE VIII. Integral momentum spectrum of cosmic-ray muons. The quoted errors include the statistical errors of the main body of data and the errors accrued in determining the absolute flux.

Momentum (GeV)	Flux [(m <sup>2</sup> sr sec) <sup>-1</sup> ]	
	75°	30°
50	$(4.08 \pm 0.21) \times 10^{-1}$	$(5.22 \pm 0.35) \times 10^{-1}$
63	$(2.81 \pm 0.14) \times 10^{-1}$	$(3.20 \pm 0.22) \times 10^{-1}$
80	$(1.91 \pm 0.10) \times 10^{-1}$	$(1.94 \pm 0.13) \times 10^{-1}$
100	$(1.31 \pm 0.07) \times 10^{-1}$	$(1.22 \pm 0.08) \times 10^{-1}$
125	$(8.82 \pm 0.50) \times 10^{-2}$	$(7.78 \pm 0.54) \times 10^{-2}$
160	$(5.55 \pm 0.32) \times 10^{-2}$	$(4.56 \pm 0.33) \times 10^{-2}$
200	$(3.74 \pm 0.23) \times 10^{-2}$	$(2.78 \pm 0.21) \times 10^{-2}$
250	$(2.50 \pm 0.16) \times 10^{-2}$	$(1.67 \pm 0.14) \times 10^{-2}$
400	$(9.37 \pm 0.74) \times 10^{-3}$	$(6.43 \pm 0.65) \times 10^{-3}$

culated simply as the ratio of measured muons to the total of measured muons and lost muons.

Table VII lists the momentum distribution of the hand-scanned events corrected for aperture dependence as before. The total numbers of aperture corrected muons over 50 GeV were then calculated for each roll, and these numbers were corrected for the measuring efficiency as also indicated in the table. The integral fluxes of muons above 50 GeV were then calculated for the two angles using these fully corrected numbers of muons and the average trigger rates and deadtime trigger efficiencies found in Table VI and the spectrometer's aperture at infinite momentum found in Table I. The values found for these fluxes are

$$F(50 \text{ GeV}, 30^\circ) = 0.522 \pm 0.035 \text{ (m}^2 \text{ sr sec)}^{-1},$$

$$F(50 \text{ GeV}, 75^\circ) = 0.393 \pm 0.020 \text{ (m}^2 \text{ sr sec)}^{-1}.$$

TABLE IX. Differential momentum spectrum of cosmic-ray muons. The quoted errors are point-to-point errors only, arising from statistical fluctuations in the main body of data. If the error on any particular point is desired, or the fluxes between the two angles is to be compared, the normalization errors of 5.2% and 6.7% for the 75° and 30° data, respectively, must be included.

Momentum (GeV)	Flux [(m <sup>2</sup> sr sec GeV) <sup>-1</sup> ]	
	75°	30°
55.9	$(9.98 \pm 0.24) \times 10^{-3}$	$(1.58 \pm 0.031) \times 10^{-2}$
70.6	$(5.41 \pm 0.12) \times 10^{-3}$	$(7.49 \pm 0.15) \times 10^{-3}$
89.0	$(3.07 \pm 0.08) \times 10^{-3}$	$(3.64 \pm 0.09) \times 10^{-3}$
111.3	$(1.74 \pm 0.054) \times 10^{-3}$	$(1.80 \pm 0.055) \times 10^{-3}$
140.6	$(9.50 \pm 0.33) \times 10^{-4}$	$(9.31 \pm 0.33) \times 10^{-4}$
178.1	$(4.60 \pm 0.21) \times 10^{-4}$	$(4.50 \pm 0.21) \times 10^{-4}$
222.6	$(2.52 \pm 0.13) \times 10^{-4}$	$(2.25 \pm 0.13) \times 10^{-4}$
309.9	$(1.09 \pm 0.052) \times 10^{-4}$	$(7.09 \pm 0.43) \times 10^{-5}$
1067	$(2.99 \pm 0.18) \times 10^{-6}$	$(2.04 \pm 0.15) \times 10^{-6}$

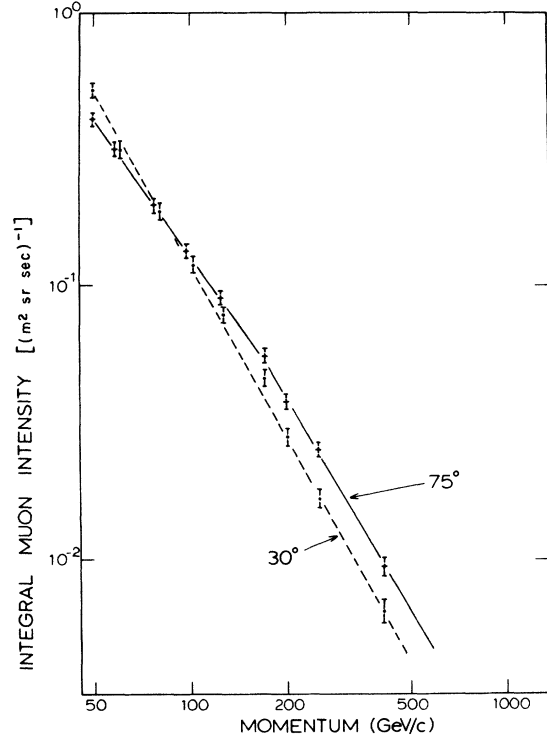


FIG. 7. Integral muon spectra at 30° and 75°.

Because of the finite width of the spectrometer's angular acceptance and the strong angular dependence of the muon flux at inclined angles, the effective angle of the spectrometer is a function of momentum when it is pointed at 75°. At low energies, muon energy loss and muon decay in passing through the atmosphere cause the muon flux to drop off as the zenith angle is increased in the vicinity of 75°, and therefore the flux of low-energy muons observed by our spectrometer when pointed at 75° will be the same as the flux observed by a spectrometer with infinitely narrow angular acceptance but pointed at some angle less than 75°. Putting this slightly differently, the finite angular acceptance of the spectrometer causes the measured flux at 75° to be greater than the actual flux at 75° for muons of low energy. Of course, for muons of high energy, the flux is increasing rather than decreasing as a function of zenith angle in the vicinity of 75°, and the finite angular acceptance of the spectrometer makes the effective angle of measurement larger than 75° or, equivalently, the measured flux at 75° smaller than the actual flux. Correction factors which convert the measured flux to the actual flux at 75° can be calculated for muons of any momentum if the angular and momentum dependence of the muon flux is known. We have calculated such correction

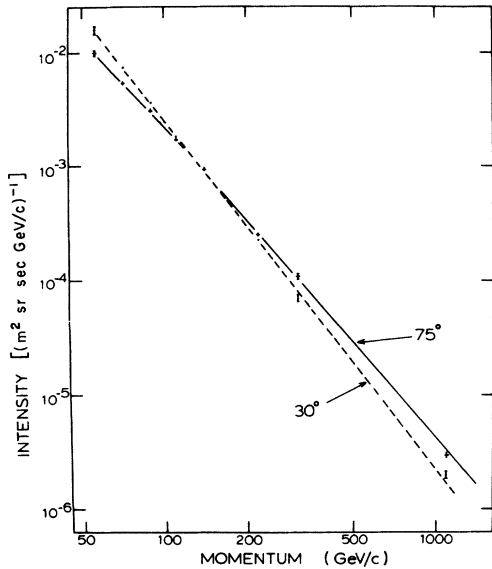


FIG. 8. Differential muon spectra at 30° and 75°.

factors on the assumption that the muon flux is described by a  $\sec\theta'$  dependence with a critical energy of 92 GeV and with appropriate treatment of muon energy loss and decay. The resulting correction factors are not strongly affected by the inaccuracies or the choice of parameters in such a simple model of the muon flux and, since the correction factors are small, this procedure of finding the true flux from the measured flux is

TABLE X. Recent spectrometer measurements of the muon charge ratio above 100 GeV.

SLAC <sup>a</sup>	1.24 ± 0.04
Durham <sup>b</sup>	1.26 ± 0.016
Durham <sup>c</sup>	1.32 ± 0.03
Kiel <sup>d</sup>	1.307 ± 0.017
Erevan <sup>e</sup>	1.25
BNL (this result)	1.23 ± 0.03

<sup>a</sup>R. J. Decoster *et al.*, *Lett. Nuovo Cimento* **12**, 239 (1975).

<sup>b</sup>J. M. Baxendale, C. J. Hume, and M. G. Thompson, *J. Phys. G* **1**, 781 (1975).

<sup>c</sup>J. M. Baxendale *et al.*, in *Proceedings of the Thirteenth International Conference on Cosmic Rays, Denver, 1973* (Ref. 2), Vol. III, p. 2011.

<sup>d</sup>K. Carstensen *et al.*, in *Proceedings of the Thirteenth International Conference on Cosmic Rays, Denver, 1973* (Ref. 2), Vol. III, p. 2082.

<sup>e</sup>T. L. Asatiani *et al.*, in *Proceedings of the Thirteenth International Conference on Cosmic Rays, Denver, 1973* (Ref. 2), Vol. III, p. 2024.

not expected to bias our results.

Using the absolute fluxes given in the last subsection, the automatically measured data were normalized, and then the 75° data were corrected for the finite angular acceptance of the spectrometer. The resulting integral and differential muon spectra are given in Tables VIII and IX and displayed in Figs. 7 and 8, respectively.

#### IV. CONCLUSIONS

##### A. Muon charge ratio

A survey of recent spectrometer measurements of the muon charge ratio in the energy range from 100 GeV to about 2 TeV reveals some scatter of the data. However, the errors of the results gathered in Table X are statistical only, and do not reflect the uncertainty in the fairly large aperture corrections which were made by most authors. It seems therefore that the results are compatible, and the charge ratio in the energy range  $\geq 100$  GeV is most likely between 1.25 and 1.30.

The result of the underground measurements of the Utah group for muon energies in the range 1–8 TeV may also be consistent too with such an average. Their earlier result<sup>4</sup> for the charge ratio was 1.30, while a later recalculation<sup>5</sup> based on the same data where the charge ratio was a fitted parameter gave as its value 1.37.

It is interesting to compare the measured charge ratio of cosmic-ray muons in the energy range covered in this experiment with the value derived theoretically. Although there is a long history of such calculations, only now do we have sufficiently extensive and reliable data on the basic hadron interactions at correspondingly high energies, obtained at the CERN intersecting storage rings (ISR), so that a comparison of the results of the calculations and of the measurements can be meaningful.

Recent calculations yield results for the charge ratio significantly higher than the value of 1.23 obtained in our experiment, and than the "world average" of recent spectrometer measurements which is less than 1.30. Adair<sup>6</sup> obtained in his calculation a value of 1.53 as a conservative minimum. The results of Erlykin *et al.*,<sup>7</sup> corrected by us using latest ISR data as input, is consistent with Adair's value. Hoffman<sup>8</sup> calculated a charge ratio of  $1.45 \pm 0.15$  for 200-GeV muons.

A recent measurement<sup>9</sup> of the charge ratio of muons produced by 400-GeV protons from the Fermilab accelerator on a copper target is quite relevant to the cosmic-ray muon charge ratio problem. The charge ratio deduced from these

measurements for muons produced in air by protons having a cosmic-ray-like energy spectrum and assuming scaling in the fragmentation region is  $1.66 \pm 0.09$ . For an 11% neutron content in the incident beam the muon charge ratio becomes then  $1.49 \pm 0.08$ , in good agreement with the calculations mentioned above, but in a poor agreement with the data.

It is then interesting to consider the consequences of the large discrepancies which seem to exist then between the calculated and observed muon charge ratios at energies of several hundred GeV. The relevant aspects of pion production in hadronic interactions are well understood, and were measured at energies close to the energies important to the muon problem. Uncertainties in the kaon flux are not significant, and since kaons produce a larger  $\mu^+/\mu^-$  ratio than pions, only a production of kaons less than that expected could push the predicted muon charge ratio toward that which is observed. Even the extreme assumption of no kaon production at all is not sufficient to reconcile theory with experiment. Since meson production measurements at the highest available energies cover only proton-proton collisions, the largest uncertainty of the calculations lies perhaps in their assumptions concerning nuclear effects, which is also the reason why the predictions cannot be made reliably for muon energies below 100 GeV. Aside from the various assumptions of particle interaction properties used in the calculation, the violation of which would be most interesting, the assumed composition of the primary radiation also has a clear effect on the calculated muon charge ratio. And it does seem that a consistent picture is growing around the possibility that the proportion of neutrons in the cosmic rays shifts markedly with energy. If the conventional low-energy primary composition remained constant up to energies per nucleon of several times  $10^{12}$  eV, and the resulting neutron/proton ratio of 0.10 actually would yield an integral muon charge ratio of 1.53 at 200 GeV, then the actual neutron/proton ratio implied by the measured muon charge ratio of 1.28 can be calculated as follows. Let  $r_p$  be the muon charge ratio generated by an incident flux of pure protons,  $R$  be the observed muon charge ratio,  $f$  be the fraction of incident nucleons that are free (necessarily protons), and let  $b$  be the fraction of incident nucleons that are bound in nuclei (assumed to be half protons and half neutrons). We have then the following relation:

$$R = \frac{\frac{1}{2}b + fw_+}{\frac{1}{2}b + fw_-},$$

where

$$w_+ = r_p/(1+r_p), \quad w_- = 1/(1+r_p),$$

where it is implicitly assumed that the nucleons bound in nuclei are not affected significantly by coherent nuclear effects within the incident nucleus. The values  $b=0.22$ ,  $R=1.53$ , obtained by Adair<sup>6</sup> imply that  $r_p=1.73$ . Solving now for the value of  $f$ , we obtain

$$f = \frac{R-1}{(w_+ - w_-)(1+R)},$$

which for  $w_+=0.634$  and  $R=1.28$ , the value obtained in this experiment for muons with energy  $E \geq 200$  GeV, yields  $f=0.46$  and  $b=0.54$ . We see, therefore, that the measured value of 1.28 for the muon charge ratio implies that approximately one-half of all primary nucleons are bound in nuclei, and then a quarter of all primary nucleons are neutrons, or that the neutron/proton ratio equals a third.

Several direct measurements of the primary composition are now available which are sensitive up to energies per nucleon of almost  $10^{11}$  eV, while measurements of protons and  $\alpha$  particles extend to even higher energies.<sup>10</sup> Although there are factors of 2 and 3 between some of the elemental abundances determined by these different measurements, it is interesting to note that they all indicate significantly flatter spectra for several heavy elements, most notably iron, than is measured for the proton spectrum. In fact, all of the measurements are consistent with an increasing heavy-element abundance compared to hydrogen which would produce a neutron/proton ratio of 0.33 at energies of several thousand GeV per nucleon.

Since a neutron/proton ratio of 0.33 implies that one-half of all nucleons will be bound in nuclei, we might hope that nuclear effects, arising within the incident nuclei during atmospheric collisions, might manifest themselves in other details of the muon flux besides the muon charge ratio. If this were the case, observation of these details would serve either to confirm or discredit the charge-ratio evidence for changes in the primary composition.

#### B. Angular dependence

We have calculated the expected zenith-angle dependence of the muon flux according to a conventional model of hadronic interactions in the atmosphere, and have evaluated how changes in the model parameters affect the results. As can be seen from Fig. 9, a graph of the logarithm of the ratio of the muon intensity at  $75^\circ$  to the intensity at  $30^\circ$  versus the logarithm of the momentum, the predictions of our model for an incident flux of

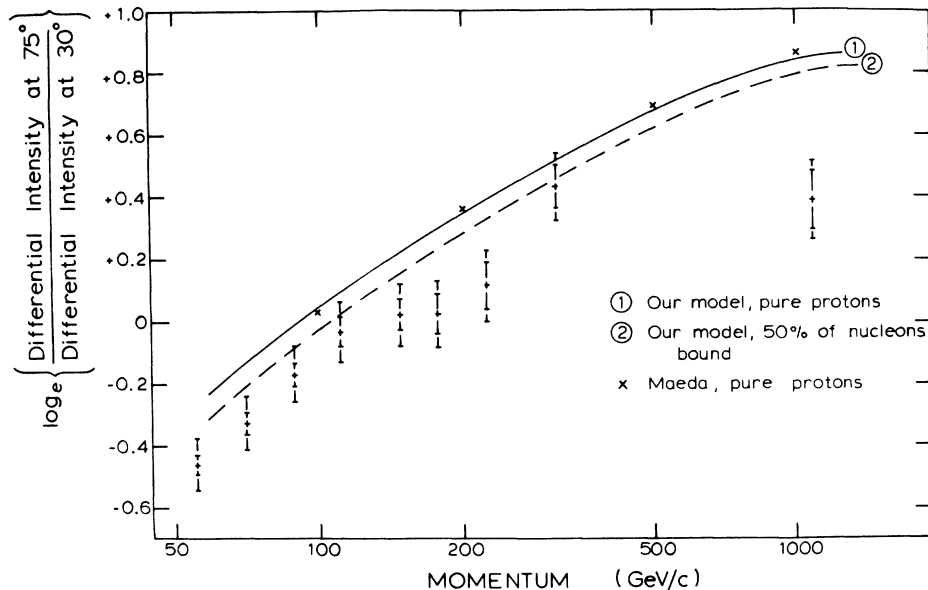


FIG. 9. Predicted (curves 1 and 2) and observed ratios of muon intensity at 75° and 30° as a function of the momentum. The smaller error bars represent the statistical errors while the larger bars include the normalization error.

pure protons fall appreciably above the experimental data. If we consider all muons above 100 GeV, we find that the measured ratio of the integral muon intensities at 75° and 30° is  $R_\theta = 1.07 \pm 0.09$ , where the error includes the normalization error. The prediction for a pure proton flux is 1.22 with an uncertainty of 0.01. Varying such parameters as the meson and nucleon attenuation lengths and the kaon/total meson production ratio within conceivable limits does nothing to remove the discrepancy, and we are forced to look beyond a simple incident flux of pure unbound nucleons for a resolution.

Since the initial interaction of even vertically incident nuclei will take place very high in the atmosphere where the probability of meson decay and hence muon production is large, the muons originating from these initial interactions should exhibit a less pronounced zenith-angle dependence than muons arising from "ordinary" collisions distributed deeper in the atmosphere. If a mechanism existed whereby meson production was effectively increased in the collisions of incident nuclei, then the reduced angular dependence of the muons arising from these collisions might be expected to make itself felt by reducing the angular dependence of the total muon spectrum.

Such a mechanism does in fact exist. "Spectator nucleons" belonging to an interacting incident nucleus but not directly involved in the high-energy interaction can nevertheless become excited by the debris of the interaction and decay emitting

mesons. Since such mesons are likely to have low energies in the frame of the incident nucleus, their distribution in the lab frame will be peaked toward large  $x$ , and their weight function will tend to be large. The production of such "spectator mesons" then provides a possible mechanism for increasing the effective meson yield from the interactions of incident nuclei. We have constructed a simple model of such a process and found that, in fact, significant effects on the angular dependence of the muon flux can occur, as can be seen from the difference between the curves labeled 1 and 2 in Fig. 9. The curve labeled 1 shows the result of our calculations for the case when all incident nucleons are considered to be free protons. It can be seen that there is good agreement between these predictions and the independent results of Maeda<sup>11</sup> which are also shown. The curve labeled 2 is the result of considering 50% of the incident nucleons to be bound in nuclei. Although the agreement of this curve with the data is not perfect, the effect of binding an appreciable fraction of the incident nucleons clearly pushes the predictions in the right direction. Again, considering all muons above 100 GeV, this nuclear model predicts that the ratio of the integral muon intensities at 75° and 30° should be 1.15, to be compared with our observed value of  $1.07 \pm 0.09$ . The results of our muon charge-ratio and angular-distribution measurements tend therefore to confirm the hypothesis that the composition of the primary cosmic rays continues its low-energy

shift toward an increasing proportion of heavy elements, at least up to nucleon energies of about  $10^{13}$  eV. Whether this trend continues yet further, and whether heavy elements, particularly iron, become the dominant components of the cosmic rays in an energy-per-nucleon sense, even as they already are in a total-energy-per-particle sense at low energy, is a particularly interesting question. Measurements of the size spectrum of extensive air showers seem to indicate that iron cannot hold the flat spectrum it displays at low energies past nucleon energies of  $10^{14}$  eV or so, because otherwise the size spectrum would need to be flatter than it appears to be. But do the spectra of the heavy elements simply steepen and become parallel to the spectrum of protons, or do they in fact become cut off? At nucleon energies above about  $10^{16}$  eV, heavy nuclei trapped in the galaxy should become photodisintegrated by head-on collisions with starlight photons. Nuclei of extragalactic origin, however, would not be eliminated so effectively by photodisintegration and, hence, the extension of primary composition measurements to nucleon energies of  $10^{16}$  eV might shed light on the origin of these very-high-energy particles.

#### ACKNOWLEDGMENTS

We have greatly benefited from discussion with R. K. Adair. We thank L. B. Leipuner and L. W. Smith for their help in designing the apparatus and useful discussions, and B. J. Higgs, who participated in the setting up of the spectrometer and in the early experimental runs.

We would like to express our special appreciation to A. Gangamella, who has admirably carried out the main task in assembling the large spectrometer.

#### APPENDIX: A MODEL OF MUON GENERATION IN THE ATMOSPHERE

We have considered a specific model of cosmic-ray muon generation in the atmosphere which predicts the energy and zenith angular dependence of the muon flux reaching the earth. Our model is conventional in that it assumes muon production takes place through the decays of pions and kaons, and that the production of these mesons in the collisions of incident primary nucleons with nuclei of the air can be understood in terms of production cross sections measured at proton accelerators along with appropriate assumptions concerning the character of nuclear effects at high energies. We have chosen to implement our model in the form of a Monte Carlo computer program which follows individual primary particles

in a semidetailed fashion through their cascades of meson producing collisions, the possible production of muons through the decay of these mesons, and the subsequent energy loss and possible decay which the muons undergo before reaching the ground.

We assume that a portion of the incoming nucleons are free protons and that a portion are nucleons bound in heavy nuclei. For simplicity, we assume that all the heavy nuclei are  $\alpha$  particles, but we believe that none of the nuclear effects which are important and which we consider will depend strongly on this assumption. We assume that the ratio of free protons to bound nucleons does not vary as a function of energy in the energy range of interest and that the energy spectrum can be represented by the expression  $dN/dE = AE^{-\gamma}$ , where  $\gamma = 2.67$ .

Since secondary particles produced in the cascade following an interaction of a primary particle can be considered to rejoin the primary spectrum, we have chosen to account for the effects of secondary particles by using appropriate attenuation lengths for the primary particles throughout our calculations. In this, we depart from a detailed treatment of the interactions of each individual particle, but presume that such interactions are considered implicitly by our choice of attenuation lengths. We use a nucleon attenuation length of  $120 \text{ g/cm}^2$  and a meson attenuation length of  $140 \text{ g/cm}^2$ .

Incident free protons are handled separately in our model, so we shall describe their treatment separately here. We treat the proton attenuation length as a mean free path and at the point of interaction in the atmosphere, a meson spectrum is generated with the following properties: The energy spectrum of the mesons, in units of the Feynman variable  $x$ , is taken as  $\exp(-8x)$ , where  $x = E_m/E_N$ , where  $E_m$  is the meson energy and  $E_N$  is the nucleon energy. For each collision, 2.16 mesons are generated on average by the program, which is much less than the total average charged multiplicity which would be about 9, since only the pions produced in the forward fragmentation region contribute to the muon flux.

The mesons are followed through the atmosphere until they either interact with a mean free path of  $140 \text{ g/cm}^2$  to account for meson regeneration in subsequent collisions, or until they decay to muons in the appropriately dilated lifetime. If the mesons interact, they are eliminated from the calculation; if they decay to muons, the muons are then followed along their path to the surface. In the course of this traverse, their possible elimination by decay and their energy loss by ionization is considered.

The ratio of kaons to pions is taken as 0.15 to follow the ratio of the weight function as computed from the ISR data. The effective kaon flux is then calculated as 0.75 times the production flux where the effective flux is considered to decay into muons and neutrinos in a two-body decay. We believe that these numbers approximate the contributions of neutral kaons and the many-body decays of charged kaons adequately for our purposes.

Incident  $\alpha$  particles, on the other hand, are treated as follows: We presume that the first interaction of an  $\alpha$  particle can be defined by an attenuation length one-fourth as large as the nucleon attenuation length, that is, an attenuation length of 30 g/cm<sup>2</sup>. We again treat this attenuation length as a mean free path and assume that a single nucleon in the  $\alpha$  will interact with a target nucleus in a manner unaffected by the presence of its three companions. After the interaction, however, the spectator nucleons of the  $\alpha$  particle are presumed to have a certain probability for interacting with the debris of the nucleon which undergoes the high-energy interaction and may then be excited to a state such that a pion is emitted. As a matter of definition, the excited state is presumed to have the unique mass of 1238 MeV and the decay pion is emitted isotropically in the center of the mass of that state. The excited state is also assumed to have the same total energy as the parent nucleon and the spectator pions produced in its decay then have a relatively large weight function of about 0.126 per pion. We assume that two spectator pions are produced on average in each  $\alpha$  particle interaction,  $\frac{2}{3}$  of these being charged, and we follow the charged ones to pick up their possible decay to muons in the same manner as previously described.

The energy loss that these spectator nucleons suffer through pion emission, charged or not, is properly accounted for, and whether or not the spectator nucleon became excited, it is followed from the point of  $\alpha$  interaction to its subsequent interaction with another atmospheric nucleus. During this period, it is treated as a free nucleon, and its production of mesons is treated in the same manner as outlined for the production of mesons by free protons above.

The nucleons in a heavy nucleus (in this case, the  $\alpha$  particle) will possess Fermi momentum, which can affect the course of their interactions to some extent. The effects are small, but we have included the Fermi momentum in a plausible approximation as a matter of completeness. We presume that the velocity of the nucleons in the nucleus can be described adequately by the relations:

$$v = p/m, \text{ where } dN/dp = A \exp(-p^2/p_0^2),$$

where  $p$  is nearly the momentum of the nucleon in the nucleus,  $p_0$  is taken as a characteristic momentum of 200 MeV/c,  $m$  is the nucleon mass, and  $A$  is the normalization constant.

We then assume that the probability of interaction of the first nucleon is proportional to  $v + c$ , where  $v$  is the velocity in the direction of the laboratory  $\alpha$  particle motion. This gives the nucleon an effective energy  $E_p = E_0(1 + v)$  and, to conserve energy, the energies of each spectator nucleon is then taken as  $E_s = E_0(1 - v/3)$ , where  $E_0$  is the mean energy per nucleon of the  $\alpha$  particle. Since the probability of interaction is greater if  $v$  is positive, the mean energy of the first nucleon to interact is somewhat greater than  $E_0$  and the mean energy of the spectator nucleons (without consideration of pion emission) will be a little less than  $E_0$ .

\*Work performed under the auspices of the U. S. Energy Research and Development Administration.

<sup>1</sup>R. K. Adair and H. Kasha, in *Muon Physics*, edited by V. W. Hughes and C. S. Wu (Academic, New York, 1977), Vol. 1, p. 323-385.

<sup>2</sup>R. W. Flint and W. F. Nash, *Acta Phys. Acad. Scien. Hung.* **29**, Suppl. 4, 99, 263 (1970); S. M. Flatté *et al.*, *Phys. Lett.* **35B**, 345 (1975); M. S. Abdel-Monem *et al.*, in *Proceedings of the Thirteenth International Conference on Cosmic Rays, Denver, 1973* (University of Denver, Denver, Colorado, 1973), Vol. III, p. 1811; C. A. Ayre *et al.*, *ibid.*, p. 1754; R. H. Burnett *et al.*, *ibid.*, p. 1864, and *Phys. Rev. Lett.* **30**, 937 (1973); O. C. Allkofer and H. Jokish, *Nuovo Cimento* **15A**, 371 (1973).

<sup>3</sup>S. Bennett and K. Greisen, *Phys. Rev.* **124**, 6 (1961).

<sup>4</sup>C. A. Ayre *et al.*, in *Proceedings of the Thirteenth*

*International Conference on Cosmic Rays, Denver, 1973* (Ref. 2), p. 1822.

<sup>5</sup>G. K. Ashley, J. W. Keuffel, and M. O. Larson, *Phys. Rev. D* **12**, 20 (1975).

<sup>6</sup>R. K. Adair, *Phys. Rev. Lett.* **33**, 115 (1974).

<sup>7</sup>A. D. Erlykin, L. K. Ng, and A. W. Wolfendale, *J. Phys. A* **7**, 2059 (1974); **7**, 2074 (1974).

<sup>8</sup>H. J. Hoffman, *Phys. Rev. D* **12**, 82 (1975).

<sup>9</sup>R. K. Adair *et al.*, *Phys. Rev. Lett.* **39**, 112 (1977).

<sup>10</sup>R. K. Balasubramanian and J. F. Ormes, *Astrophys. J.* **186**, 109 (1973); L. H. Smith *et al.*, *ibid.* **180**, 987 (1973); E. Juliusson, *ibid.* **191**, 331 (1974); M. J. Ryan *et al.*, *Phys. Rev. Lett.* **28**, 985 (1972).

<sup>11</sup>K. Maeda, in *Proceedings of the Sixth Interamerican Seminar on Cosmic Rays, La Paz, Bolivia, 1970* (Universidad Major de San Andrés, La Paz, 1970), p. 847.